Journal of Sound and Vibration (2000) **236**(4), 657–682
doi:10.1006/jsvi.2000.3037, available online at http://www.idealibrary.com on IDEAL®

FINITE ELEMENT MODELLING OF MAGNETIC CONSTRAINED LAYER DAMPING

M. RUZZENE AND J. OH

Mechanical Engineering Department, Catholic University of America, Washington, DC 20064, *U.S.A.*

AND

A. BAZ

Mechanical Engineering Department, University of Maryland, College Park, MD 20742, *U.S.A.*

(*Received* 30 *June* 1999, *and in final form* 15 *March* 2000)

The performance of a new treatment consisting of integrated arrays of constrained visco elastic damping layers passively controlled by a specially arranged network of permanent magnets is evaluated. The interaction between the magnets and the viscoelastic layers aims at enhancing the energy dissipation characteristics of the damping treatments. In this manner, it would be possible to manufacture structures that are light in weight and are capable of meeting strict constraints on structural vibration when subjected to unavoidable disturbances. In this paper, a finite element model is developed to study the interactions between the permanent magnets and their influence on the dynamic behavior of treated beams. The model is used to develop a thorough understanding of the basic phenomena governing the operation of this new class of smart magnetic constrained layer damping (MCLD) treatments. The performance characteristics of the MCLD are determined for fully treated beams and compared with the corresponding performance of conventional passive constrained layer damping (PCLD). Such a comparison is used to determine the merits and limitations of the proposed MCLD treatments.

1. INTRODUCTION

Passive constrained layer damping (PCLD) treatments have been successfully utilized, for many years, to damp out the vibration of flexible structures ranging from simple beams to complex space structures [1]. However, the effectiveness of these treatments has been limited to a narrow operating range because of the significant variation of the properties of damping materials with temperature and frequency. Hence, treatments that are a hybrid between active and passive damping have been considered as viable alternatives to the conventional passive damping treatments. Such hybrid treatments aim at using active control mechanisms to augment the passive damping and to compensate for its performance degradation with temperature or frequency. Among the commonly used hybrid treatments are the active constrained layer damping (ACLD) treatments [2–5], and the active piezoelectric-damping composites (APDC) [6–8]. In the ACLD treatments the piezo-film is actively strained in a manner to enhance the shear deformation of the viscoelastic damping layer in response to the vibration of the base structure. In the APDC treatments an array of piezo-ceramic rods embedded across the thickness of a viscoelastic polymeric matrix is electrically activated to control the compressional damping characteristics of the matrix directly bonded to the vibrating structure.

0022-460X/00/390657 + 26 $35.00/0

Although the ACLD and APDC treatments have proven to be very successful in damping out structural vibration, they require the use of piezoelectric films, amplifiers and control circuits. As simplicity, reliability, practicality and effectiveness are our ultimate goal in controlling the vibration and noise; the concept of the magnetic constrained layer damping (MCLD) is introduced to eliminate the need for these films, associated circuitry as well as any external energy [9, 10].

In this paper, a finite element model is developed to fully understand the phenomena governing the operation of the MCLD treatments and to evaluate their effectiveness in controlling the vibration of flexible beams as compared to conventional PCLD. In particular, the model describes the interaction between the dynamics of beams and the magnetic field generated by magnetic constraining layers. The model is used to predict the stiffness and mass matrices of the beam/MCLD system as functions of the properties of the permanent magnets, viscoelastic cores and base beam. This analysis is guided by the theory of magneto-elasticity developed by Moon [11] and Miya *et al.* [12, 13] for untreated and undamped base structures.

The paper is organized in five sections and one appendix. In section 1, a brief introduction is given. In section 2, the concept of the MCLD treatment is presented. The finite element formulation for the magnetic domain and structural vibration is given in section 3. The performance of beams fully treated with the MCLD treatment is presented in section 4 with comparisons with the performance of beams treated with conventional PCLD treatments. In section 5, the conclusions of the present study are summarized.

2. CONCEPT OF MAGNETIC CONSTRAINED LAYER DAMPING (MCLD)

The concept of the MCLD can best be understood by considering the schematic representation of the PCLD treatment shown in Figure 1. The undeflected configuration of the structure/PCLD system is shown in Figure 1(a) whereas Figure 1(b) shows the deflected configuration under the action of an external bending moment. Due to such loading, shear strains γ_T and γ_B are induced in the top and bottom viscoelastic layers respectively. Increasing these shear strains is essential to enhancing the energy dissipation characteristics of the damping treatment. A preferred way for increasing the shear strains is to replace the conventional constraining layers by properly arranged and designed magnetic layers.

Figure 2 shows two possible arrangements of the magnetic constraining layers, where the inter-layer interaction is either in repulsion as in Figure 2(a) or in attraction as in Figure 2(b). Figure 2(a) shows that MCLD, with layers in repulsion, have strains γ_{Tr} and γ_{Br} which are lower than the strains γ_T and γ_B of conventional PCLD treatments. Hence, it is not beneficial to arrange the magnetic layers in repulsion because of their low energy dissipation

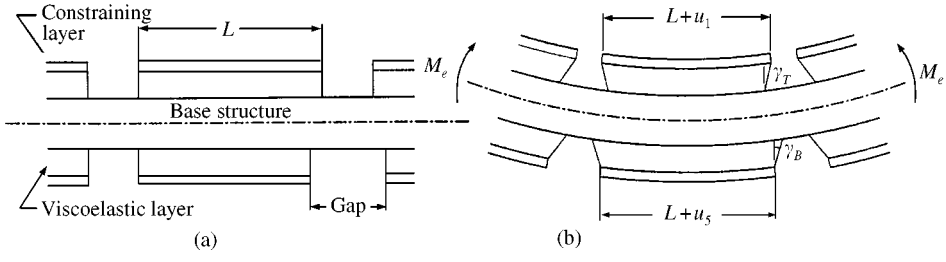

Figure 1. Conventional multi-segment passive constrained layer damping: (a) undeflected configuration and (b) deflected configuration.

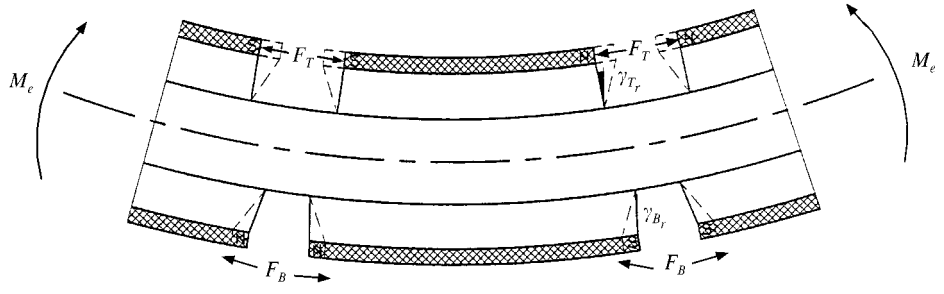

(a)

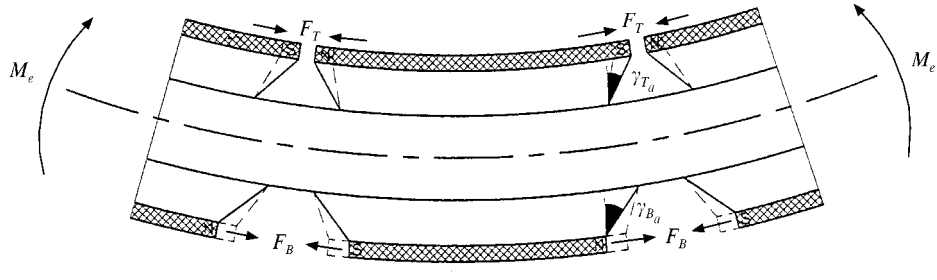

(b)

Figure 2. Possible arrangements of the magnetic constrained layer damping: (a) layers in repulsion and (b) layer in attraction (PCLD-dashed lines and MCLD-solid lines)

characteristics. This is in spite of the fact that such MCLD arrangement induces in-plane tensile loads in the base structure which tend to enhance its stiffness.

It is evident however that the shear strains γ_{Ta} and γ_{Ba} resulting from the attraction arrangement are much higher than the strains γ_{Tr} and γ_{Br} of the repulsion arrangement. Note also that the strains γ_{Ta} and γ_{Ba} exceed the strains γ_T and γ_B of the conventional PCLD treatment. Therefore, significant improvement of the damping characteristics can be achieved by using MCLD treatments with magnetic layers in attraction.

Such improved damping exists in ACLD and APDC treatments but at the expense of the complexities associated with the use of piezo-sensors, piezo-actuators, control circuitry and/or external energy. Hence, the use of the MCLD improves the damping characteristics of conventional PCLD treatments in a much simpler and efficient way. Hybrid configuration of the ACLD and MCLD can however be viable when the self-damped characteristics of the MCLD are to be enhanced in order to compensate, for example, for performance degradation due to changes in the operating temperature or to improve/shape the frequency characteristics of the composite assembly.

3. FINITE ELEMENT MODELLING OF BEAMS WITH MCLD TREATMENT

3.1. MAGNETIC FINITE ELEMENT

The magnetic properties of the region surrounding the permanent magnets in the MCLD are obtained by the numerical computation of the magnetic vector potential.

3.1.1. *Mathematical formulation*

In static magnetic problems, the relations between the magnetic field **H**, the magnetic induction **B**, the current density **j** and the magnetization **M** are given by Maxwell's equation [14]:

$$\text{curl } \mathbf{H} = \mathbf{j}, \qquad \text{div } \mathbf{B} = 0, \tag{1, 2}$$

and

$$\mathbf{B} = \mu_0(\mathbf{H} + \mathbf{M}), \tag{3}$$

where μ_0 is the permeability in vacuum.

The relation between **M** and **H** in regions occupied by isotropic materials can be expressed as

$$\mathbf{M} = (\mu_r - 1)\mathbf{H}, \tag{4}$$

where μ_r is the relative permeability of the material.

Permanent magnets are generally made of anisotropic material and therefore the magnetization **M** is given by

$$\mathbf{M} = M(B_m)\mathbf{m}, \tag{5}$$

m being the direction of the magnetization and B_m the induction in that direction.

The magnetic properties of a given magnetic domain can be determined by minimizing its magnetic energy [15], which is defined as

$$E_m = \int_V \left(\int_0^B \mathbf{H} \cdot \mathrm{d}\mathbf{B} - \mathbf{j} \cdot \mathbf{A} \right) \mathrm{d}V, \tag{6}$$

where V is the volume of the region where the magnetic properties have to be evaluated.

In equation (6), **A** is the magnetic potential, defined as

$$\mathbf{B} = \text{curl } \mathbf{A}. \tag{7}$$

For beams lying in the x–z plane, the vector potential **A** is perpendicular to the x–y plane:

$$\mathbf{A} = A(x, y) \cdot \mathbf{k}, \tag{8}$$

k being the unit vector in the z direction. From equations (7) and (8), the magnetic induction **B**, becomes

$$\mathbf{B} = B_x(x, y)\,\mathbf{i} + B_y(x, y)\,\mathbf{j} = -\frac{\partial}{\partial y}(A(x, y))\,\mathbf{i} + \frac{\partial}{\partial y}(A(x, y))\,\mathbf{j} \tag{9}$$

and the magnetization **M** is

$$\mathbf{M}(B_m) = M(B_x \cos \alpha_m + B_y \sin \alpha_m)\,\mathbf{m}, \tag{10}$$

where α_m is the angle between the direction of magnetization **m** and the x-axis.

In the MCLD case, the analysed region does not contain any current windings, then current density **j** in equations (1) and (6) is equal to zero and the magnetic field is generated

only by the presence of permanent magnets. The total magnetic energy is hence the sum of the energy due to anisotropic material $E_{m_{an}}$, i.e., the permanent magnets:

$$E_{m_{an}} = b \int_G \left(\frac{1}{\mu_0} \int_0^B \mathbf{B} \cdot \mathrm{d}\mathbf{B} - \int_0^B \mathbf{M} \cdot \mathrm{d}\mathbf{B} \right) \mathrm{d}x \, \mathrm{d}y$$

$$= b \int_G \left(\frac{1}{2\mu_0} \left[\left(\frac{\partial A}{\partial x} \right)^2 + \left(\frac{\partial A}{\partial y} \right)^2 \right] - \int_0^B \mathbf{M}(\xi) \, \mathrm{d}\xi \right) \mathrm{d}x \, \mathrm{d}y \tag{11}$$

and of the energy $E_{m_{is}}$ given by isotropic non-magnetic material, i.e., base beam, viscoelastic cores and surrounding air, such that

$$E_{m_{is}} = b \int_G \left(\int_0^B \frac{\xi}{\mu_0 \mu_r(\xi)} \, \mathrm{d}\xi \right) \mathrm{d}x \, \mathrm{d}y \tag{12}$$

In equations (11) and (12), b is the width of the off plane region and G is the area of the considered region on the x, y plane.

Hence, the total magnetic energy of the domain is given by

$$E_m = E_{m_{an}} + E_{m_{is}}. \tag{13}$$

3.1.2. *Finite element formulation*

Equations (11) and (12) express the magnetic energy as a function of the magnetic potential **A**. The magnetic properties of the magnetic domain will be determined by finding the values of the potential **A** that make E_m stationary. Accordingly, the region is divided into triangular finite elements, where the potential **A** is assumed to be linear [16]:

$$A^e(x, y) = b_1 + b_2 \cdot x + b_3 \cdot y. \tag{14}$$

Equation (14) can be written in the matrix form

$$A^e(x, y) = [1 \;\; x \;\; y] \begin{Bmatrix} b_1 \\ b_2 \\ b_3 \end{Bmatrix}. \tag{15}$$

The element vector potential $A^e(x, y)$ can be expressed in terms of the nodal potentials A_i ($i = 1, 2, 3$):

$$A^e(x, y) = [1 \;\; x \;\; y] \, [D^{-1}] \begin{Bmatrix} A_1 \\ A_2 \\ A_3 \end{Bmatrix} = [N_m(x, y)] \, \{A^e\}. \tag{16}$$

where the matrix $[D]$, defined as

$$[D] = \begin{bmatrix} 1 & x_1 & y_1 \\ 1 & x_2 & y_2 \\ 1 & x_3 & y_3 \end{bmatrix}, \tag{17}$$

contains the nodal co-ordinates $[x_i, y_i]$ ($i = 1, 2, 3$). Also in equation (16), $[N_m(x, y)]$ is the matrix of the magnetic shape functions.

From equation (16), the contribution to the magnetic energy from the eth element of the anisotropic material is given by

$$E^e_{m_{an}} = \frac{1}{2}\{A^e\}^T[K_m]\{A^e\} - \{Mg\}\{A^e\}, \tag{18}$$

where $[K_m]$ is the magnetic stiffness matrix, given by

$$[K_m] = \frac{b}{2\mu_0}\int_G \{[N_m]_x^T[N_m]_x + [N^m]_y^T[N_m]_y\}\,\mathrm{d}x\,\mathrm{d}y. \tag{19}$$

The subscripts x and y in equation (19) denote partial differentiation with respect to x and y respectively. It can be shown that the partial derivatives of the shape functions considered in equation (19) do not depend on x and y, therefore the magnetic stiffness matrix reduces to

$$[K_m] = \frac{b}{2\mu_0}([N_m]_x^T[N_m]_x + [N_m]_y^T[N_m]_y)\alpha^e \tag{20}$$

where α^e is the area of the eth element of the magnetic domain.

In equation (18), $\{Mg\}$ is the magnetization vector, defined as

$$\{Mg\} = b\cdot\alpha^e\cdot M(B_m)[\cos\alpha_m \;\; \sin\alpha_m]\begin{bmatrix}[N_m]_x\\ [N_m]_y\end{bmatrix}\{A^e\}. \tag{21}$$

The contribution to the energy of the magnetic domain by an element of the isotropic material is obtained by setting the magnetization vector in equation (18) to zero.

The values of the magnetic potential minimizing the magnetic energy are obtained by partially differentiating equation (18) with respect to the nodal potentials:

$$\frac{\partial E_m}{\partial\{A^e\}} = 0. \tag{22}$$

This yields the following equation that describes the properties of the magnetic domain:

$$[K_m]\{A^e\} = \{Mg\}. \tag{23}$$

Equation (23) is generally non-linear in the potentials because of the non-linear magnetization characteristic of the permanent magnets and of the relative permeability of the isotropic materials, as described by equation (11) and (12). If appropriate constant values for the magnetization and for the relative permeability are assumed, then the equations can be linearized and an approximate solution can be easily found.

3.1.3. *Static magnetic force*

The static magnetic forces $F_m^{(st)}$ are determined by applying the virtual work principle [17]. If s is the line of action of the magnetic forces, then $F_m^{(st)}$ can be determined from

$$F_m^{(st)} = -\frac{\partial E_m}{\partial s} = -\frac{\partial}{\partial s}\left(\int_V\left(\int_B \mathbf{H}\cdot\mathrm{d}\mathbf{B}\right)\mathrm{d}V\right). \tag{24}$$

During small translations in the s direction of the movable parts, which belong to the magnetic domain, the magnetic potential is assumed to remain constant. Therefore, considering the expression for the magnetic stiffness matrix given by equation (20), equation (24) can be rewritten as

$$F_m^{(st)} = \frac{1}{2}\{A^e\}^T \frac{\partial}{\partial s}([K_m])\{A^e\}. \tag{25}$$

The derivative of the magnetic stiffness matrix is determined by considering the expression of the derivative of the shape function $[N_m]$ with respect to x and y. In particular, it can be shown that

$$[N_m]_x = \frac{1}{2\alpha^e}[y_2 - y_3 \;\; y_3 - y_1 \;\; y_1 - y_2] = \frac{1}{2\alpha^e}[Y] \tag{26}$$

and

$$[N_m]_y = \frac{1}{2\alpha^e}[x_3 - x_2 \;\; x_1 - x_3 \;\; x_2 - x_1] = \frac{1}{2\alpha^e}[X], \tag{27}$$

where x_i and y_i are the nodal co-ordinates.

Assuming that the area of the element α^e remains constant, then the magnetic force can be expressed as

$$F_m^{(st)} = -\frac{b}{8\mu_0\alpha^e}\{A^e\}^T \frac{\partial}{\partial s}([Y]^T[Y] + [X]^T[X])\{A^e\}. \tag{28}$$

The x and y components of the magnetic force are determined from equation (28) as

$$F_{m_y}^{(st)} = -\frac{b}{8\mu_0\alpha^e}\{A^e\}^T \frac{\partial}{\partial y}([Y]^T[Y])\{A^e\} \tag{29}$$

and

$$F_{m_x}^{(st)} = -\frac{b}{8\mu_0\alpha^e}\{A^e\}^T \frac{\partial}{\partial x}([X]^T[X])\{A^e\}, \tag{30}$$

Equations (29) and (30) can be rewritten as

$$F_{m_y}^{(st)} = \{A^e\}[\Phi_y]\{A^e\}, \quad F_{m_x}^{(st)} = \{A^e\}^T[\Phi_x]\{A^e\}, \tag{31, 32}$$

where

$$[\Phi_y] = -\frac{b}{4\mu_0\alpha^e}([Y]^T[Y']), \qquad [\Phi_y] = -\frac{b}{4\mu_0\alpha^e}([X]^T[X']). \tag{33, 34}$$

In equations (33) and (34), $[Y']$ and $[X']$ are matrices containing the derivatives of the nodal co-ordinates with respect to x and y. For a given point $[x_1, y_1]$, these derivatives are given by

$$\frac{\partial y_i}{\partial x} = 0, \quad \frac{\partial x_i}{\partial x} = p, \quad \frac{\partial y_i}{\partial y} = p, \quad \frac{\partial x_i}{\partial y} = 0,$$

with $p = 1$ for the nodes belonging to a moving part of the magnetic domain and $p = 0$ for the nodes of all the other elements.

3.1.4. *Comparison with experimental data*

The prediction of the forces using the magnetic finite element model presented above are validated experimentally in this section. In particular, the simple case of two permanent magnets, made of neodymium blocks ($0{\cdot}375 \times 0{\cdot}8 \times 2{\cdot}5$ cm) with residual induction $B_r = 1{\cdot}08$ T and magnetized through their thickness, has been considered. In the finite element model, the two magnets have been divided into eight elements along the length and four elements along the thickness. Figure 3 shows the position of the magnets inside the meshed region, the geometry of the region and the magnetization vectors. The results obtained from the analysis are shown in Figures 4–6. In particular, Figure 4 displays the distribution of the magnetic vector potential over the magnetic domain. Figures 5 and 6 show the corresponding vector plots of the magnetic induction and the magnetic force acting on one magnet respectively. The x-component of the resultant force is computed by summing the contributions from all the elements and is compared with experimental measurements for different values of the gap between the permanent magnets. The comparison is made when both the magnets are arranged in attraction and repulsion. The comparison between finite element predictions and experimental measurements is presented in Figure 7. The figure shows good agreement for the case of the magnets in repulsion (Figure (7(a)). The finite element model seems to overestimate the force when the magnets are in attraction (Figure (7(b)).

3.2. STRUCTURAL FINITE ELEMENT MODEL OF THE BEAM/MCLD SYSTEM

The finite element model of a beam with magnetic constrained layer damping MCLD treatment is developed to describe the interaction between the dynamics of the plain beam,

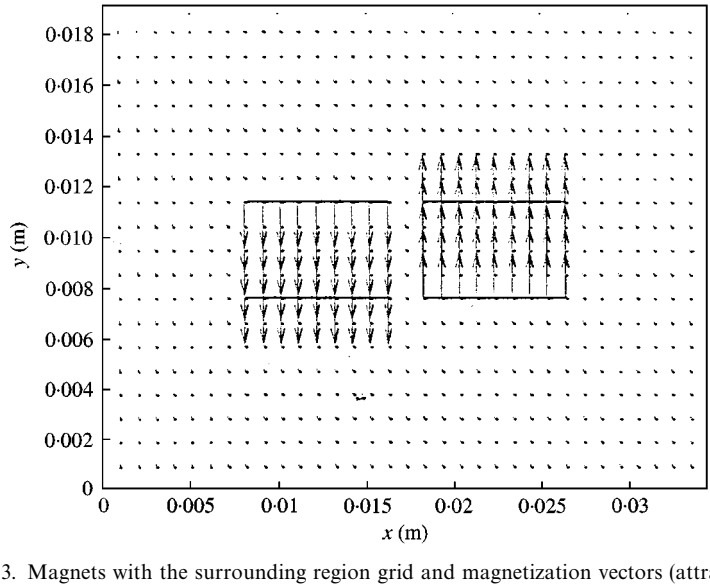

Figure 3. Magnets with the surrounding region grid and magnetization vectors (attraction).

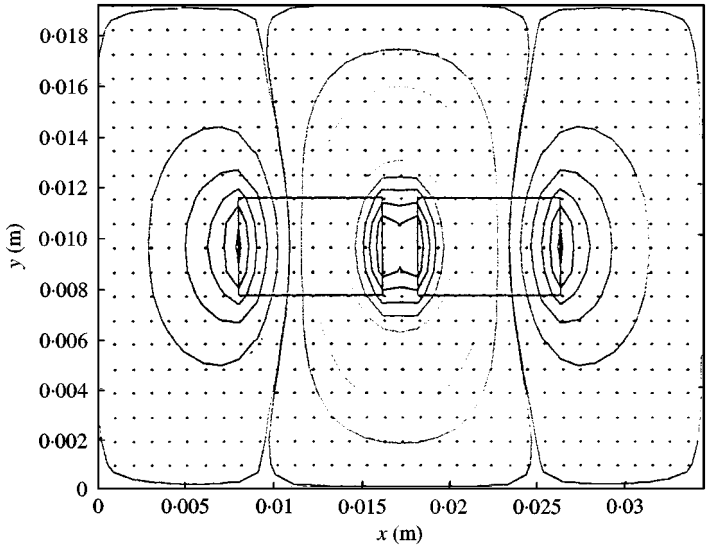

Figure 4. Magnetic potential contour lines.

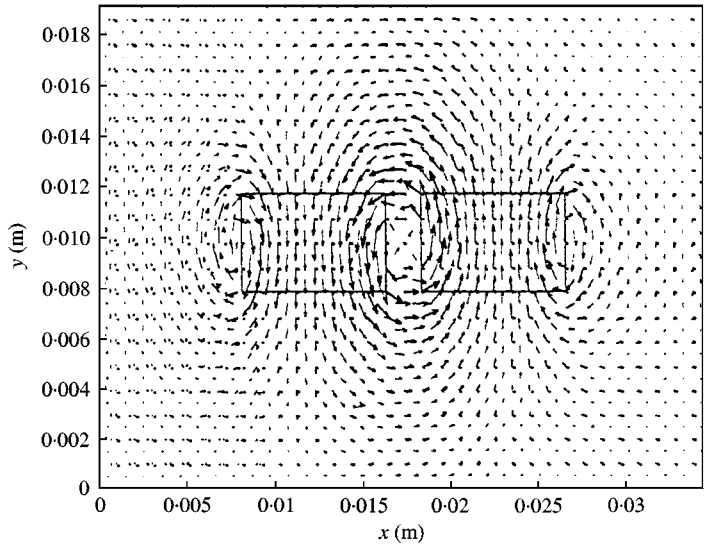

Figure 5. Magnetic induction vector plot for the configuration in Figure 1.

viscoelastic layers and constraining layers. A full and symmetric treatment of the beam is considered here.

The structural finite element model presented hereafter is coupled with the magnetic finite element model described in section 3.1.

3.2.1. *Geometry and basic kinematic assumptions*

A schematic drawing of the geometry of a beam with symmetric MCLD treatment is shown in Figure 8.

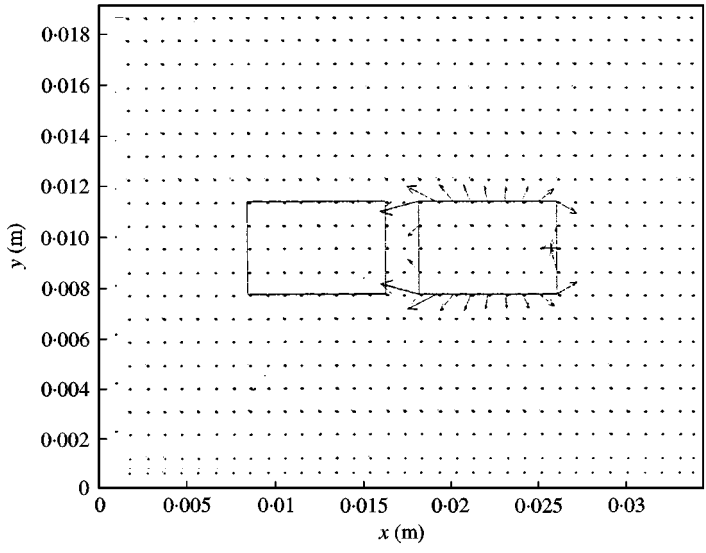

Figure 6. Magnetic force vector plot for the configuration in Figure 1.

The basic assumptions used in the formulations of the finite element are those commonly used for sandwiched beams: (1) the shear strain in the constraining layers and in the beam are negligible; (2) the longitudinal stresses in the viscoelastic cores are negligible; (3) the transverse displacements w of all points on the cross-section are assumed to be equal; (4) the viscoelastic cores dissipate energy and have a linear viscoelastic behavior, while the constraining layers and the beam are assumed to be elastic.

From the geometry of Figure 9, the shear strains in the viscoelastic cores can be expressed as

$$\gamma_2 = \frac{1}{h_2}[u_1 - u_3 + d_2 w_x], \qquad \gamma_4 = \frac{1}{h_4}[u_3 - u_5 + d_4 w_x], \tag{35a,b}$$

where u_1 and u_5 are the longitudinal deflections of the constraining layers, u_3 is the longitudinal deflection of the base beam and w_x denotes the slope of the deflection line. The parameters d_2 and d_4 are

$$d_2 = h_2 + \tfrac{1}{2}(h_1 + h_3), \qquad d_4 = h_4 + \tfrac{1}{2}(h_5 + h_3), \tag{36a,b}$$

where h_1, h_5 and h_3 are the thickness of the constraining layers and of the base beam respectively. Also h_2 and h_4 are the thickness of the viscoelastic layers.

The longitudinal deflections u_2 and u_4 of the viscoelastic cores are determined in terms of the longitudinal displacements u_1 and u_5 and of the slope of the deflection line w_x as

$$u_2 = \frac{1}{2}\left[u_1 + u_3 + \left(\frac{h_1 - h_3}{2}\right) w_x\right] \quad \text{and} \quad u_4 = \frac{1}{2}\left[u_5 + u_3 + \left(\frac{h_5 - h_3}{2}\right) w_x\right] \tag{37a,b}$$

3.2.2. *Degrees of freedom and shape functions*

The MCLD elements considered here are one-dimensional elements, bounded by two nodal points. Each node has four degrees of freedom to describe the longitudinal

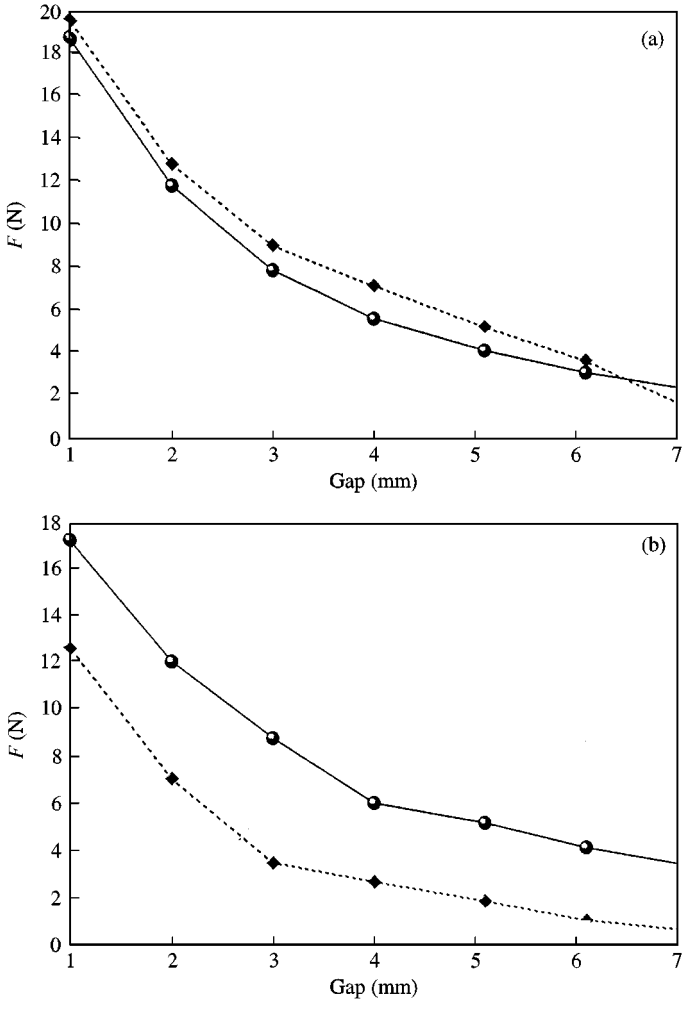

Figure 7. Magnetic force versus the distance between the permanent magnets: comparison with experimental data for magnets in (a) repulsion and (b) attraction; (●, theory; ◆, experiment).

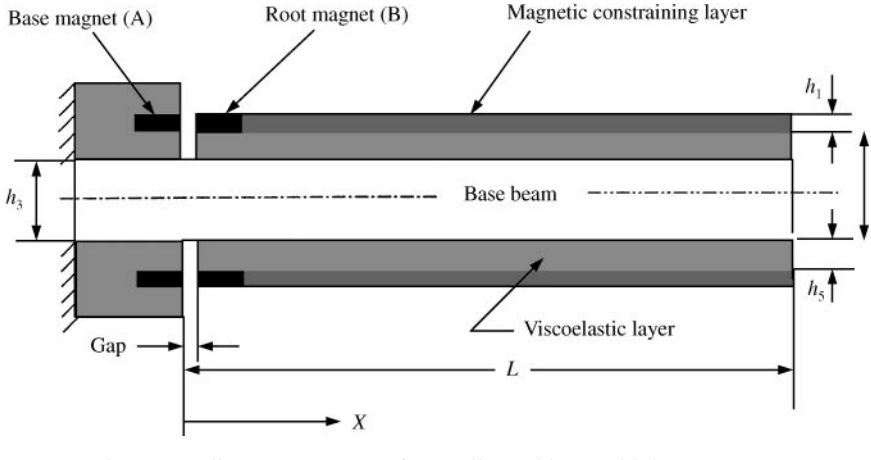

Figure 8. Full MCLD treatment for cantilevered beam with base magnets.

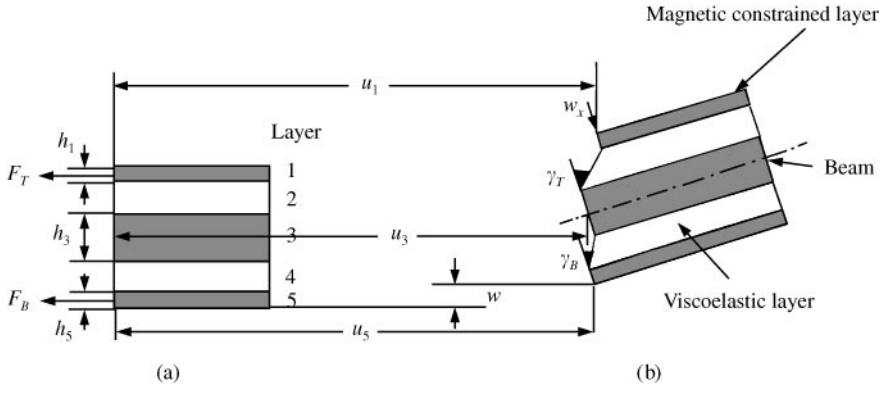

Figure 9. Schematic drawing of the deflections and forces acting on the MCLD: (a) undeflected and (b) deflected configuration.

displacements of the two constraining layers u_1 and u_5, the longitudinal displacement of the base beam u_3, the transverse deflection w and the slope w_x. The deflection vector $\{\delta^*\}$ of each MCLD element is given by

$$\{\delta^e\} = \{u_{1i}, u_{3i}, u_{5i}, w_i, w_{xi}, u_{1j}, u_{3j}, u_{5j}, w_j, w_{xj}\}^T, \tag{38}$$

i and j denoting the left and right node respectively.

The shape functions describing the displacements over the element are assumed to be

$$u_1 = a_1x + a_2, \quad u_3 = a_3x + a_4, \quad u_5 = a_5x + a_6, \quad w = a_7x^3 + a_8x^2 + a_9x + a_{10} \tag{39}$$

Equation (39) can be expressed in a compact form as

$$\{u_1, u_3, u_5, w, w_x\}^T = [N_1, N_2, N_3, N_4, N_5]\{a_1, a_1, \ldots, a_{10}\}^T. \tag{40}$$

The constants a_i are determined in terms of the nodal displacements:

$$\{u^e\} = [T]\{a_1, a_1, \ldots, a_{10}\}^T, \tag{41}$$

where $[T]$ is a transformation matrix obtained by imposing the value of the shape functions at the boundaries of the element. The deflections at any location of the element can therefore be expressed as a function of the nodal displacements using the $[N]$ and $[T]$ matrices as follows:

$$\{u\} = [N][T^{-1}]\{\delta^e\} \tag{42}$$

where

$$[N] = [N_1, N_2, N_3, N_4, N_5] \tag{43}$$

3.2.3. *Magneto-elastic coupling*

The magnetic forces calculated using the finite element model presented in section 3.1 are applied to the nodes of the beam/MCLD element. In general, the magnetic forces have x and y components, but because of symmetry, only the x components are non-zero. Therefore, the magnetic forces are applied to the axial displacements u_1 and u_5 of the

constraining layers. These displacements affect the nodal co-ordinates of the element, which are contained in the expressions of the magnetic force (matrices $[Y]$ and $[X]$ in equations (33) and (34)). This yields

$$\begin{aligned} x_1 &= x_{1_0} + u_i, \quad x_2 = x_{2_0} + u_i, \quad x_3 = x_{3_0} + u_i, \\ y_1 &= y_{1_0} + w, \quad y_2 = y_{2_0} + w, \quad y_3 = y_{3_0} + w, \end{aligned} \tag{44}$$

where w is the transverse deflection of the beam, while u_i ($i = 1, 5$) denote the longitudinal displacement of the upper or lower constraining layers. Accordingly, the derivative of the magnetic shape functions, given by equations (26) and (27), can be rewritten as

$$[N_m]_x = \frac{1}{2\alpha^e}([Y] + \{\delta^e\}^T[\Omega_y]^T) \tag{45}$$

and

$$[N_m]_y = \frac{1}{2\alpha^e}([X] + \{\delta^e\}^T[\Omega_x]^T), \tag{46}$$

where the matrices $[\Omega_y]$ and $[\Omega_x]$ define the structural degrees of freedom that influence the y and x nodal co-ordinates of the magnetic domain. Therefore, the static expression for the magnetic force given in section 3.1.3 needs to be corrected by introducing an additional term that accounts for the fact that the permanent magnets are mounted on a vibrating structure. As mentioned above, only the x component of the magnetic force is non-zero and, according to equation (46), it can be written as

$$F_{m_x} = \{A^e\}^T([\Phi_x] + [\Phi_x^{(d)}])\{A^e\}, \tag{47}$$

where the matrix $[\Phi_x^{(d)}]$, defined as

$$[\Phi_x^{(d)}] = -\frac{b}{8\mu_0\alpha^e}([\Omega_x]\{\delta^e\}[X'] + \{X'\}^T\{\delta^e\}^T[\Omega_x]^T) \tag{48}$$

accounts for the effect of the beam vibration on the expression of the force.

Note that the magnetic force, as predicted by equation (47), is a non-linear function of the magnetic potential and the beam displacement. For small displacements about the beam's equilibrium configuration, it can be assumed that the magnetic potential remains constant during the beam vibration. Also, the magnetic forces can be linearized about the equilibrium configuration as follows:

$$F_{m_a} \cong F_{m_x}^{(st)} + \frac{\partial F_{m_x}}{\partial u_i}\bigg|_{u_i=0}^T u_i, \tag{49}$$

where $F_{m_x}^{(st)}$ is the static component of the magnetic force evaluated in section 3.1.3 and u_i denotes the longitudinal displacement of the upper or lower constraining layer.

After some manipulations, equation (49) can be written as

$$F_{m_x} \cong \{A_0^e\}^T[\Phi_x]\{A_0^e\} - \frac{-b}{4\mu_0}\{\delta^e\}^T[\Omega_x]^T[X']^T = F_{m_x}^{(st)} + F_{m_x}^{(d)}, \tag{50}$$

which includes the static component $F_{m_x}^{(m)}$ of the magnetic force as well as its dynamic component $F_{m_x}^{(d)}$, which is proportional to the nodal deflection vector $\{\delta^e\}$. In equation (50), subscript 'o' denotes the equilibrium position.

3.2.4. *Equation of motion*

The equation of motion of the beam with MCLD treatment can be obtained by applying Hamilton's principle [18]

$$\int_{t_1}^{t_2} \delta(T - U + W_m + W_e)\,\mathrm{d}t = 0, \tag{51}$$

where $\delta(\cdot)$ denote the first variation, t_1 and t_2 are the initial and final time, T and U are the total kinetic and strain energies of the element, W_e is the work done by the external loads and W_m is the work of the magnetic forces. The derivation and the expression of the total kinetic and potential energies are given in Appendix A. The work of the external loads $\{F\}$ can be expressed as

$$W_e = \{F\}\{\delta^e\}, \tag{52}$$

while the work done by the magnetic forces is given by

$$W_m = F_{m_x}^{(d)}\{b\}^T\{\delta^e\} - \frac{1}{2}F_{m_x}^{(st)}\int_0^L w_x^2\,\mathrm{d}x, \tag{53}$$

where $\{b\}$ is a vector defining the points of application of magnetic forces. Substituting the expression of the magnetic force given in equation (50) yields

$$W_m = -\{\delta^e\}^T[K_{geo}]\{\delta^e\} - \{\delta^e\}^T[K_{dm}]\{\delta^e\}, \tag{54}$$

where $[K_{geo}]$ is the geometric matrix defined as

$$[K_{geo}] = F_{m_x}^{(st)}[T^{-1}]^T\left(\int_0^L N_{4x}^T N_{4x}\,\mathrm{d}x\right)[T^{-1}]. \tag{55}$$

The geometric matrix accounts for the effect of the static term of the magnetic forces. In equation (54), the matrix $[K_{dm}]$ is the magneto-structural stiffness matrix:

$$[K_{dm}] = \frac{b}{2\mu_0\alpha^e}\{b\}[X'][\Omega_x]. \tag{56}$$

By performing the variations on the expressions of the strain and kinetic energies and on the work of the external and magnetic forces, the following equation of motion for the beam/MCLD system is obtained:

$$[M]\{\ddot{\delta}^e\} + ([K] + [K_{dm}] + [K_{geo}])\{\delta^e\} = \{F\}, \tag{57}$$

where $[M]$ and $[K]$ denote the element mass and stiffness matrices, given in Appendix A. The static magnetic interactions, corresponding to the first term in equation (54), are

applied to the longitudinal degrees of freedom of the beam and their effect is accounted for by adding a geometric stiffness matrix to the stiffness (Appendix A).

Equation (57) represents the basic equation governing the dynamic of a beam/MCLD element. Assembly of the different elements using classical finite element methods and imposing the boundary conditions gives the equation of motion of the overall beam/MCLD system. The resulting equation can be used to predict the dynamics characteristics of the system for different arrangements of the magnets on the constraining layers.

4. PERFORMANCE OF BEAMS WITH MCLD TREATMENT

4.1. MODEL OF THE PERMANENT MAGNETS AND SURROUNDING REGION

The magnetic properties of the region surrounding the permanent magnets in the base and on the constraining layers of the beam are determined using the finite element model presented in section 3.1. The magnets used for the validation of the magnetic force calculation (section 3.1.4), are considered here (neodymium blocks $0{\cdot}375 \times 0{\cdot}8 \times 2{\cdot}5$ cm, magnetized through the thickness, with residual induction $B_r = 1{\cdot}08$ T). Each magnet is divided into four elements along the length and two elements along the thickness. The dimensions of the surrounding region are adjusted in order to attain a vanishing vector potential at the boundaries and to have the magnets placed in the center so that a symmetric configuration can be preserved. Figure 10 shows the meshed region with the four magnets: the magnets are in repulsion and the gap between them is 4 mm. The predicted magnetic properties of the region are presented in Figure 11–13. Figures 12 and 13, in particular, show the position of the MCLD beam with respect o the permanent magnets.

4.2. THE BEAM MODEL

The performance of a cantilever aluminum beam, 30 cm long, 0·05 cm thick and 2·5 cm wide are evaluated. The viscoelastic and the aluminum constraining layers are 0·3125 and

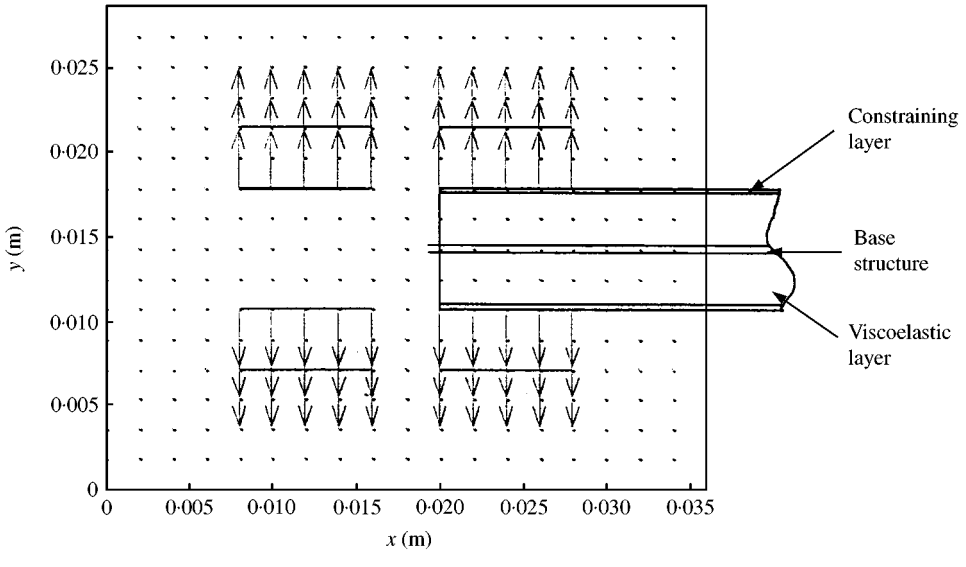

Figure 10. Mesh of the four magnets and surrounding region and magnetization vectors (4 mm gap).

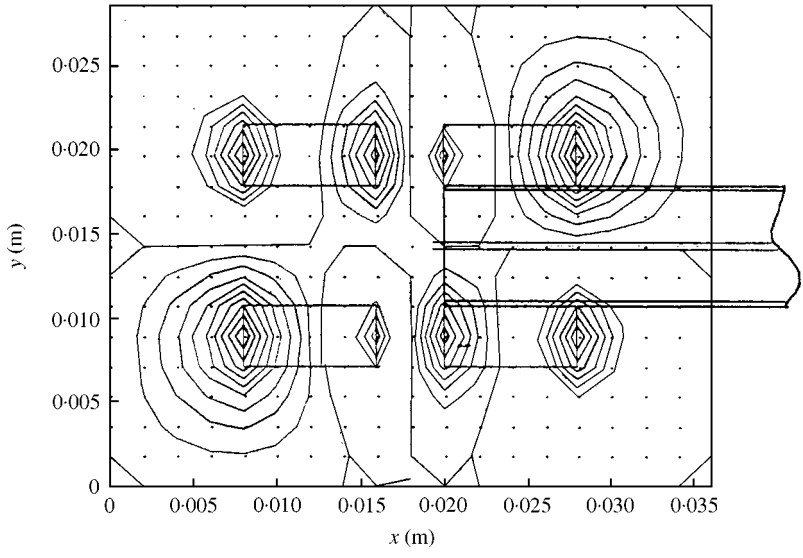

Figure 11. Magnetic potential contour lines for the configuration in Figure 7.

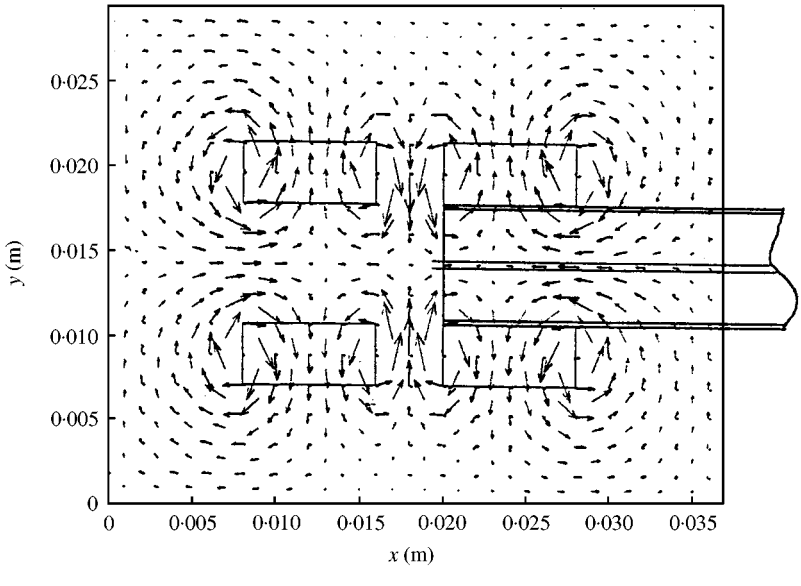

Figure 12. Vector plot of the magnetic induction for the configuration in Figure 7.

0·025 cm thick respectively. The storage modulus of the viscoelastic cores is $G' = 0{\cdot}4\text{E}6\ \text{N/m}^2$, the loss factor is $\eta = 0{\cdot}4$ and the density is $\rho = 150\ \text{kg/m}^3$.

The finite element mesh used for the magnetic analysis is also used here, for the initial part of the beam, so that the nodal magnetic forces can be applied to the constraining layers. For the remaining part, the beam is divided into 40 elements. The first three modes of the beam, without the permanent magnets, are 5·31, 74·29 and 133·81 Hz.

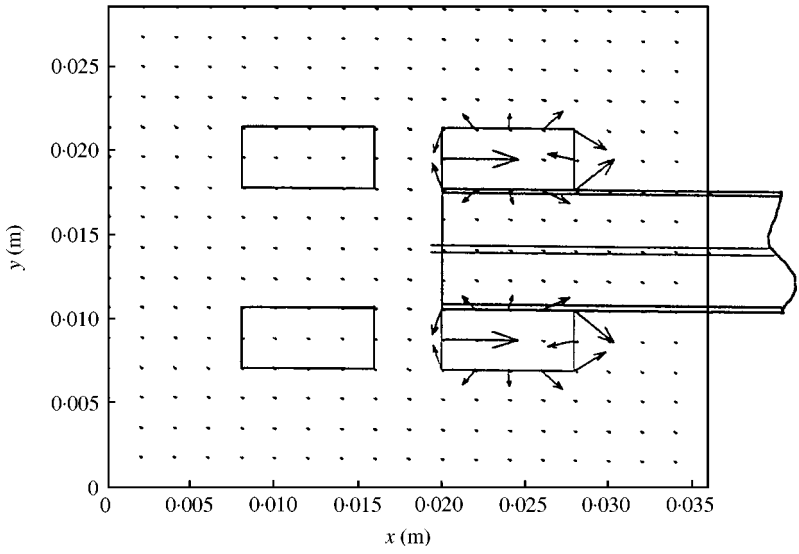

Figure 13. Vector plot of the magnetic force on the magnets on the constraining layers for the configuration in Figure 7.

4.3. BEAM WITH MAGNETS IN THE BASE AND IN THE CONSTRAINING LAYERS

The model of the beam/MCLD with magnets on the base and on the constraining layers is considered first. The response of the beam is computed for magnets arranged in attraction and repulsion. The beam is excited by a harmonic motion of its base. Three different amplitudes of the base motion are used in the analysis: $w_0 = 0{\cdot}23$, $0{\cdot}17$ and $w_0 = 0{\cdot}11$ mm. The influence of the magnetic forces on the beam tip displacement is determined for different values of the gap along the x direction: 2, 4, 6 and 18 mm. For gap width equal to 18 mm the magnetic forces become negligible and the MCLD treatment behaves like a conventional PCLD treatment.

Figure 14 shows the frequency response function of the beam with MCLD treatment for different gaps and amplitudes of the base motion, with the magnets arrange in repulsion. The presence of tensile axial loads on the beam due to the magnetic interaction increases the stiffness of the beam and reduces the shear deformation of the viscoelastic layers. Accordingly, the damping characteristics of the beam are reduced and the amplitudes of vibration are increased.

These phenomena are reversed when the magnets are arranged in attraction (Figure 15). The presence of axial compression loads reduces the first natural frequency but enhances the damping characteristics. In particular, vibration attenuation of the amplitude of the tip is observed for small gaps and high amplitudes of excitation.

Figure 16 summarizes the performance on the MCLD treatment and underlines that magnets in attraction ensures better attenuation than the conventional PCLD treatment, particularly for small gaps and high amplitudes of excitation.

4.4. BEAM WITH MAGNETS IN THE BASE ONLY

The performance of the treatment is also studied when only two magnets in the base of the beam are considered. Two blocks of ferromagnetic material (relative permeability $\mu_r = 1000$)

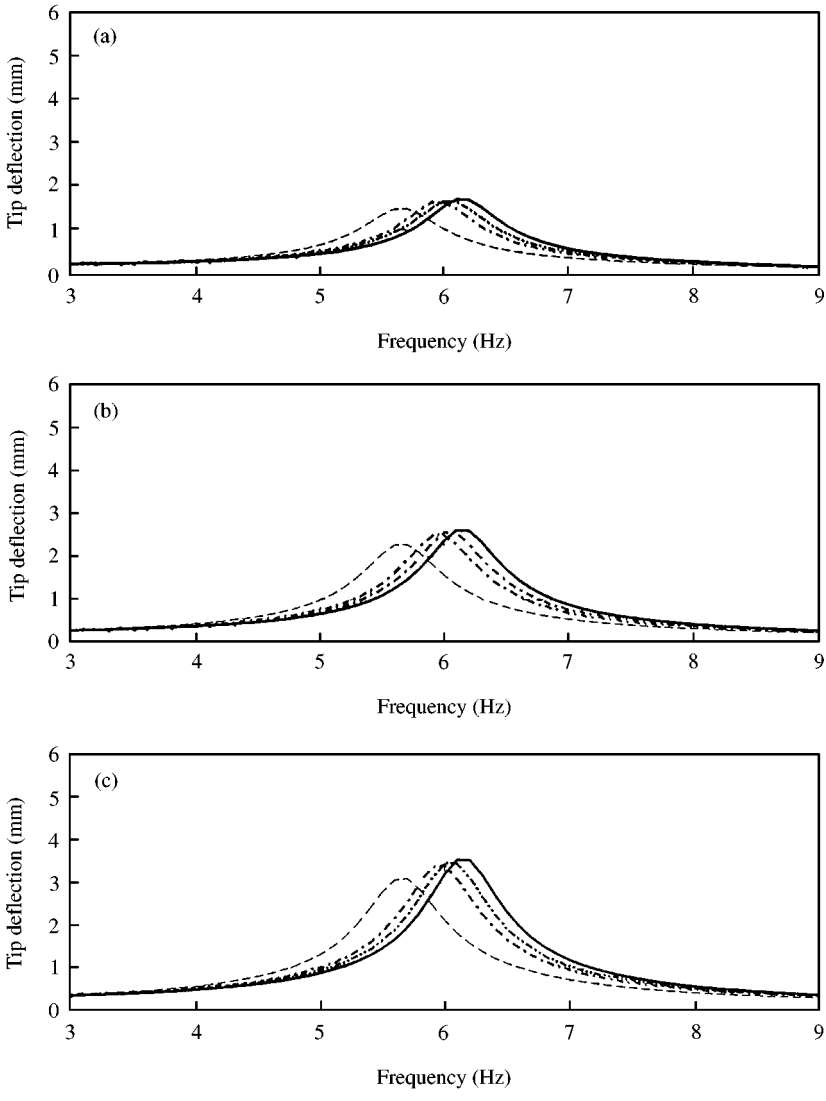

Figure 14. Frequency response of the beam tip for magnets in repulsion with different amplitudes of base excitation. (a) $w_0 = 0{\cdot}11$ mm, (b) $w_0 = 0{\cdot}17$ mm, (c) $w_0 = 0{\cdot}23$ mm (——, 2 mm gap; – · · –, 4 mm gap; – · –, 6 mm gap; –; 18 mm gap).

are used instead of the magnets of the previous arrangements. In this configuration, the design of the MCLD is simplified and the interactions result only in attraction forces.

Figure 17 shows the configuration of the magnetic region with the two magnets and the blocks of ferromagnetic material. The resulting magnetic properties of the region are presented in Figure 17–20. The response of the MCLD treatment, in its new configuration, is again studied for different gaps and amplitudes of the base excitation. In particular, the same values of the gap and of w_0 used before are considered. The results s are presented in Figure 21. This new configuration with two magnets enhances also the damping characteristics of the beam, and the performance is very similar to that obtained using four magnets in attraction.

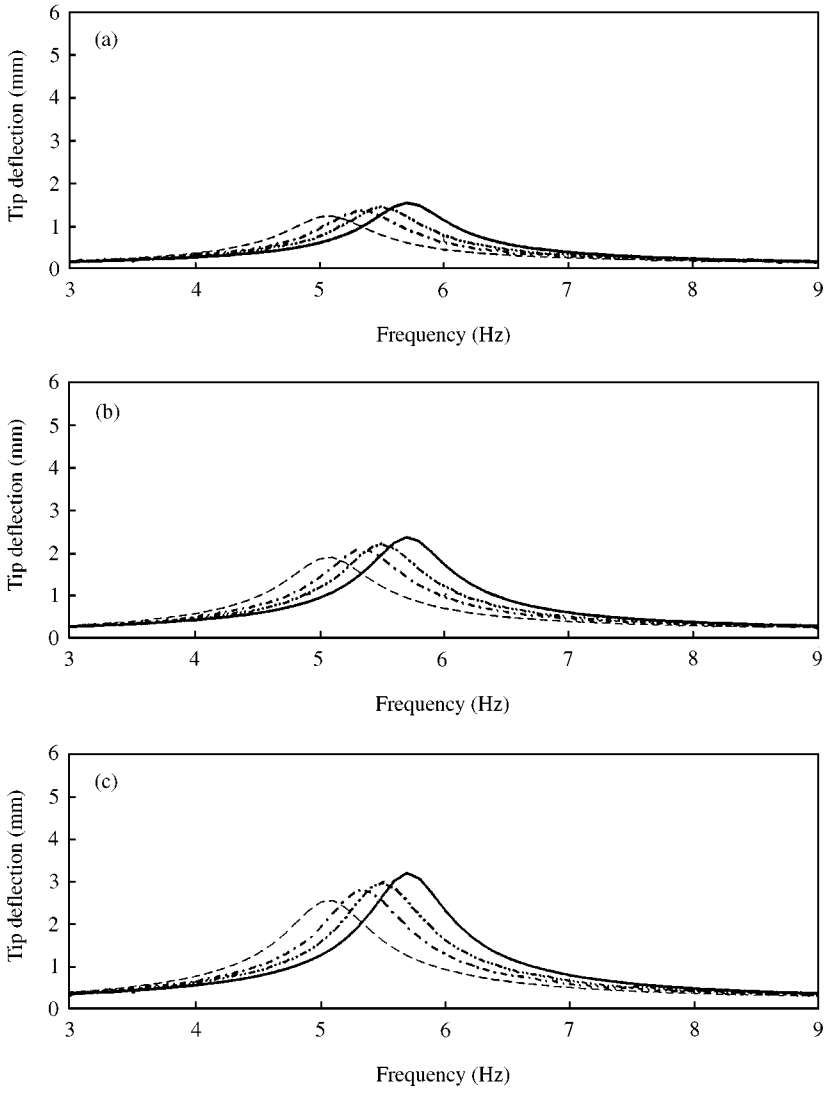

Figure 15. Frequency response of the beam tip for magnets in attraction with different amplitudes of base excitation: (a) $w_0 = 0{\cdot}11$ mm, (b) $w_0 = 0{\cdot}17$ mm, (c) $w_0 = 0{\cdot}23$ mm (——, 2 mm gap; – · · –, 4 mm gap; – · –, 6 mm gap; – – · ; 18 mm gap).

Figure 22 summarizes the effect of the gap and the base excitation on the performance of the MCLD treatment.

5. CONCLUSIONS

This paper has presented a new class of magnetic constrained layer damping (MCLD) treatments which relies in its operation on an array of viscoelastic damping layers passively controlled by a specially arranged network of permanent magnets. The proposed MCLD treatment enhances the damping characteristics of conventional PCLD treatments without

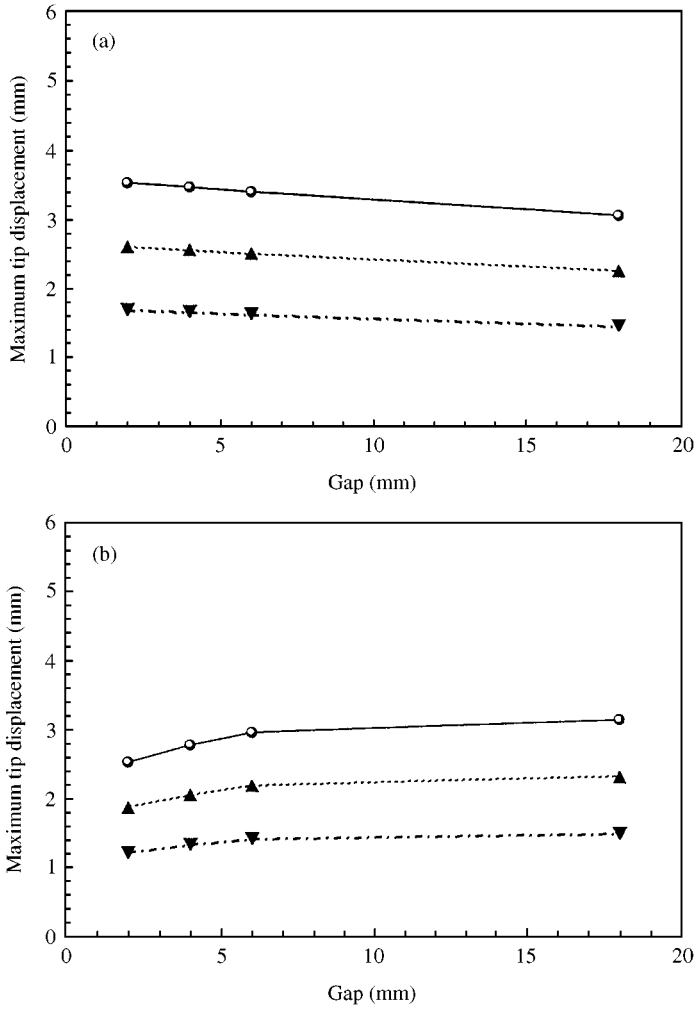

Figure 16. Effect of gap and amplitude of excitation for magnets in (a) repulsion and in (b) attraction (–●–, $w_0 = 0{\cdot}23$ mm; –▲–, $w_0 = 0{\cdot}17$ mm; –▼–, $w_0 = 0{\cdot}11$ mm).

the need for any electronic sensors, control circuitry or external energy. Such excellent feature of the MCLD makes its operation simple, reliable and efficient as compared to other surface damping treatments.

A finite element model is developed to evaluate the effectiveness of the MCLD in controlling the vibration of flexible beams. The model describes the dynamic behavior of beams and the coupling with the magnetic forces generated by the constraining layers. The model is used to predict the stiffness and mass matrices of the beam/MCLD system as functions of the properties magnets, viscoelastic cores and base beam. The response of the tip of a cantilever beam is evaluated in the frequency domain for different arrangements of the permanent magnets. The obtained results suggested that constraining layers placed in a state of magnetic attraction produce high damping characteristics and that improved structural damping is achieved by reducing the gap between neighboring layers.

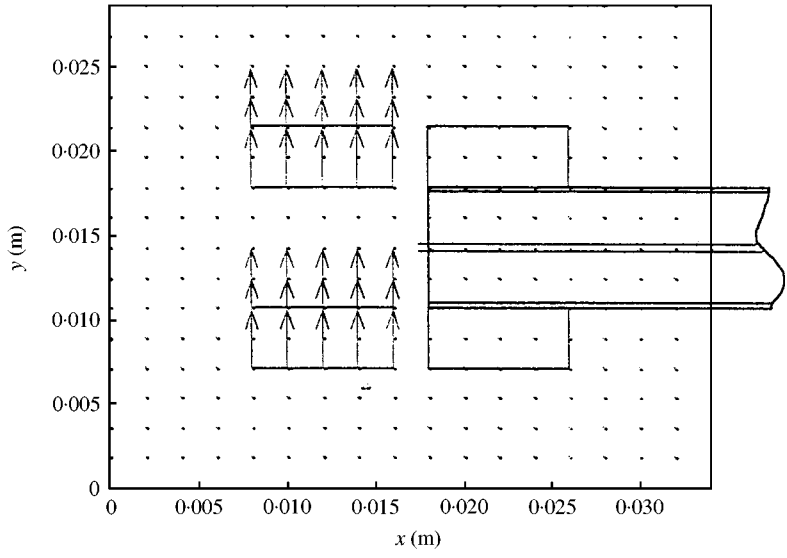

Figure 17. Mesh of a region with two permanent magnets and ferromagnetic material.

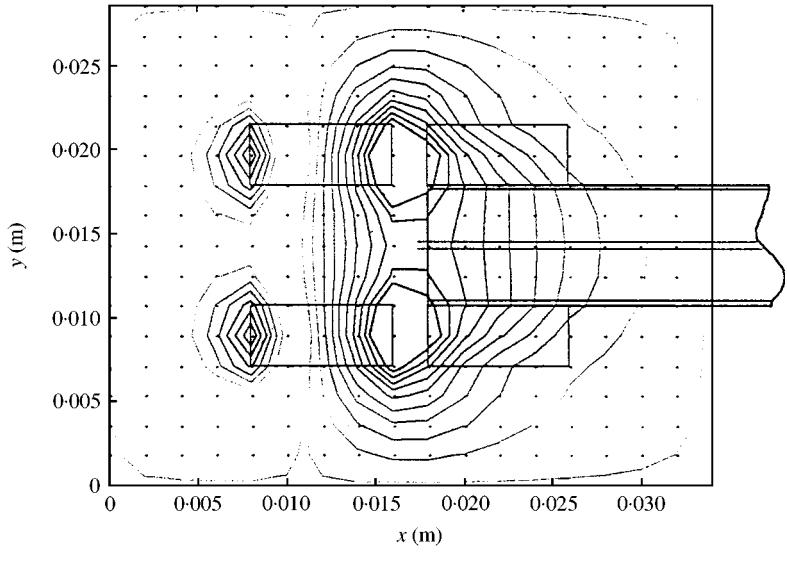

Figure 18. Magnetic vector potential contour lines.

It is important to note that a hybrid of the MCLD and ACLD treatments can be viable means for enhancing the damping characteristics of the MCLD. The hybrid configuration will be able to compensate, for example, for performance degradation due to changes in the operating temperature or to improve/shape the frequency response characteristics of the composite assembly.

Work is now in progress to optimize the performance of the MCLD, develop design guidelines and extend its application to plates and shells.

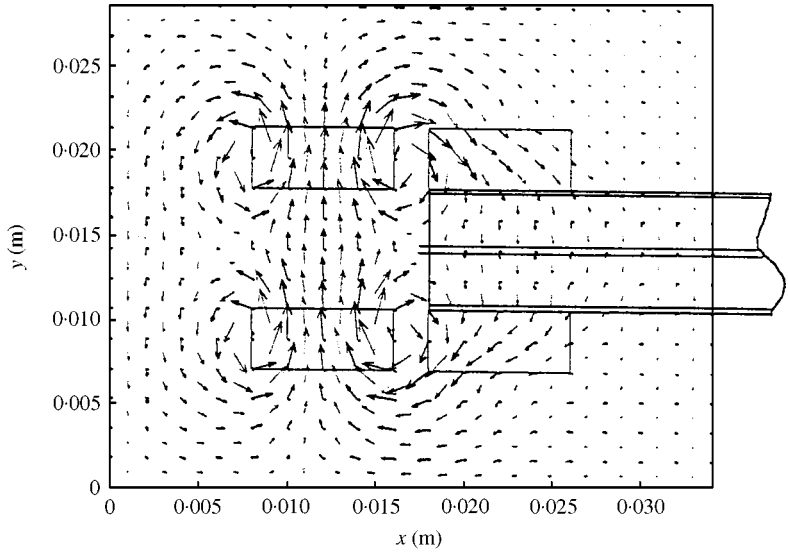

Figure 19. Vector plot of the magnetic induction.

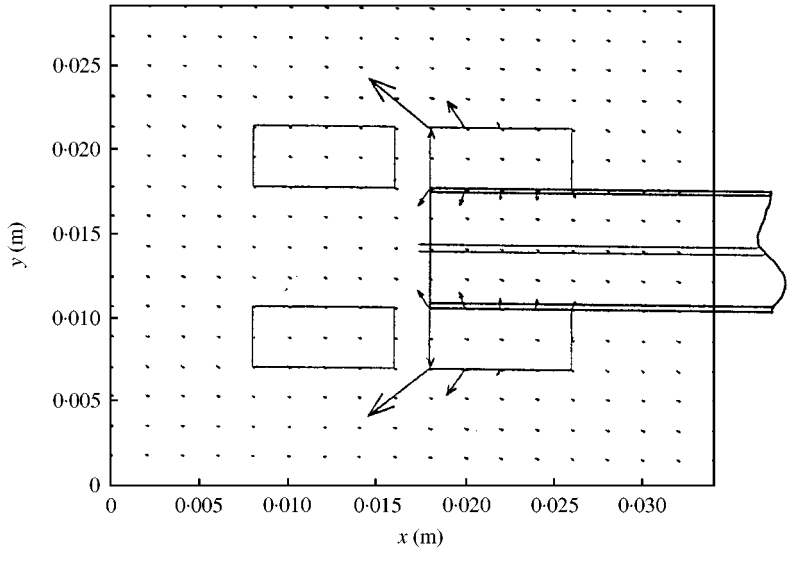

Figure 20. Vector plot of the magnetic forces on the ferromagnetic material.

ACKNOWLEDGMENTS

This work is funded by The U.S. Army Research Office (Grant number, DAAH-04-96-1-0317). Special thanks are due to Dr Gray Anderson, the technical monitor, for his invaluable technical inputs.

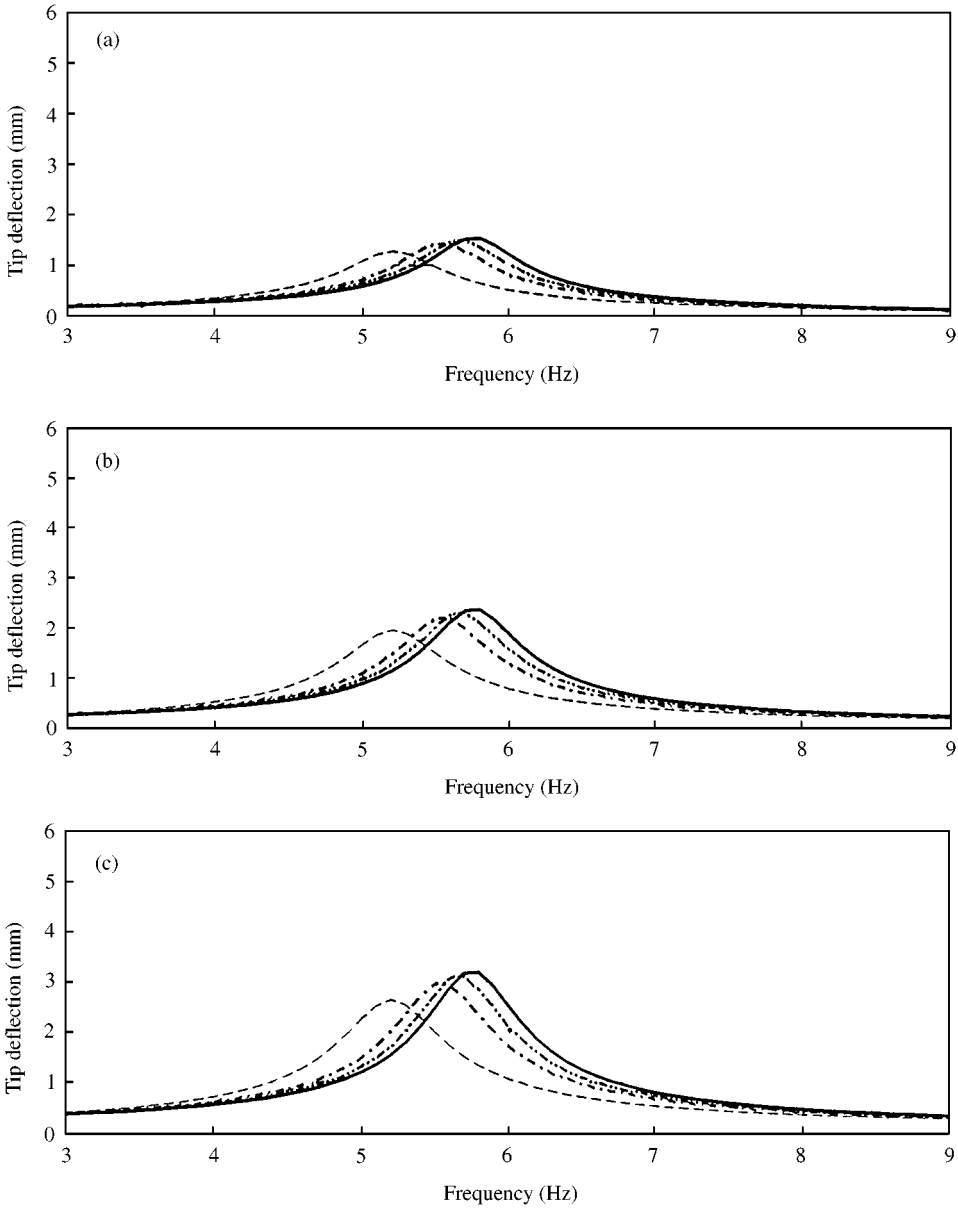

Figure 21. Frequency response of the beam tip with ferromagnetic material for different amplitudes of base excitation: (a) $w_0 = 0{\cdot}11$ mm, (b) $w_0 = 0{\cdot}17$ mm, (c) $w_0 = 0{\cdot}23$ mm (——, 2 mm gap; – · ·, 4 mm gap; – · –, 6 mm gap; – – ·, 18 mm gap).

REFERENCES

1. C. T. Sun and Y. P. Lu 1995 *Vibration Damping of Structural Elements*. Englewood Cliffs, NJ: Prentice-Hall.
2. A. Baz 1996 *U.S. Patent* #5,485,053. Active constrained layer damping.
3. A. Baz and J. Ro 1994 *Sound and Vibration Magazine* **28**, 18–21. Actively controlled constrained layer damping.
4. S. C. Haung, D. Inman and E. Austin 1996 *Journal of Smart Materials and Structures* **5**, 301–314. Some design considerations for active and passive constrained layer damping treatments.

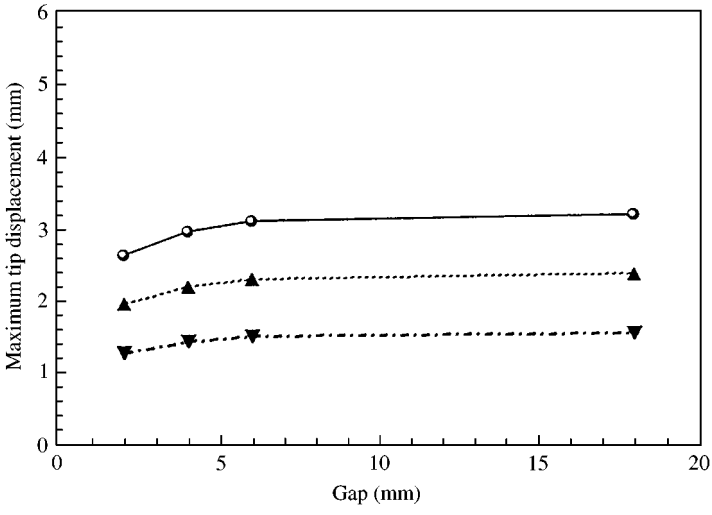

Figure 22. Effect of gap and amplitude of excitation for treatment with ferromagnetic material (–●–, $w_0 = 0{\cdot}23$ mm; –▲–, $w_0 = 0{\cdot}17$ mm; –▼–, $w_0 = 0{\cdot}11$ mm).

5. W. LIAO and K. W. WANG 1995 *Proceedings of ASME 15th Biennial Conference on Vibration and Noise*: DE Vol. 84-3, Part C, 125–142. On the active–passive hybrid vibration control actions of structures with active constrained layer treatments.
6. W. READER and D. SAUTER 1993 *Proceedings of DAMPING'93*, GBB 1–18. Piezoelectric composite for use in adaptive damping concepts.
7. R. D. GENTILMAN, F. FIORE, H. T. PHAM, K. W. FRENCH and L. J. BOWEN 1994 *Ceramic Transactions* **43**, 239–247. Fabrication and properties of 1–3 PZT polymer composites.
8. W. SHIELDS, J. RAO and A. BAZ 1998 *Journal of Smart Materials and Structures* **7**, 1–11. Control of sound radiation from a plate into an acoustic cavity using active piezoelectric damping composites.
9. A. BAZ 1997 *U.S. Patent Application.* Magnetic Constrained Layer Damping.
10. A. BAZ 1997 *Eleventh Symposium on Structural Dynamics and Control*, Blacksburg VA, 333–343. Magnetic constrained layer damping.
11. F. MOON 1984 *Magneto-Solid Mechanics.* New York: John Wiley & Sons.
12. K. MIYA, K. HARA and Y. TABATA 1980 *Nuclear Engineering and Design* **59**, 401–410. Finite element analysis of experiment on dynamic behavior of cylinder due to electromagnetic force.
13. K. MIYA and M. UESAKA 1982 *Nuclear Engineering and Design* **72**, 275–296. An application of finite element method to magnetomechanics of superconducting magnets for magnetic fusion reactors.
14. D. J. GRIFFITH 1995 *Introduction to Electrodynamic.* New Delhi: Prentice-Hall of India .
15. W. KAMMINGA 1975 *Journal of Applied Physics D* **8**, 841–855. Finite-element solution for devices with permanent magnets.
16. P. P. SILVESTER and R. L. FERRARI 1996 *Finite Elements for Electrical Engineers.* Cambridge: Cambridge University Press.
17. J. L. COULOMB and G. MEUNTER 1984 *IEEE Transactions on Magnetics* **20**, 1894–1896. Finite element implementation of virtual work principle for magnetic or electric force and torque computation.
18. L. MEIROVITCH 1967 *Analytical Methods in Vibrations.* New York: Mcmillan Publishing Co., Inc.

APPENDIX A: MASS AND STIFFNESS MATRICES

A.1. MASS MATRIX

The kinetic energy T is written as

$$T = \frac{1}{2} \sum_{j=1,3,5} \int_0^{L_j} m_j (w_t^2 + u_{t_j}^2)\, \mathrm{d}x = \frac{1}{2} \{\dot{\Delta}^e\}^T [M] [\dot{\Delta}^e\}, \tag{A.1}$$

where $[M]$ is the mass matrix given by

$$[M] = \int_0^L [N]^T [m][N]\,\mathrm{d}x, \tag{A.2}$$

and where $[N] = [N_1\ N_2\ N_3\ N_4\ N_5]$, and $[m] = \mathrm{diag}[m_1\ m_3\ m_5\ m_t\ 0]$ with $m_t = \sum_{i=1}^{5} m_i$.

A.2. STIFFNESS MATRIX

The strain energy U is written as

$$U = \frac{1}{2}\left[\int_0^{L_j}\left\{\left(\sum_{j=1,3,5} EI_j\right) w_{xx}^2 + \sum_{j=1,3,5} ES_j u_{x_j}^2\right\}\mathrm{d}x\right] + \frac{1}{2}\int_0^L \left[Gb \sum_{j=2,4} h_j \gamma_j^2\,\mathrm{d}x\right]$$

$$= \frac{1}{2}\{\Delta^e\}^T[K]\{\Delta^e\}. \tag{A.3}$$

where $[K]$ is the structural stiffness matrix given by

$$[K] = \int_0^L \{[N_{xx}]^T[B_w][N_{xx}] + [N_x]^T[B_u][N_x]\,\mathrm{d}x$$

$$+ \int_0^L Gb\{[N]^T(h_2\{B_{s2}\}^T\{B_{s2}\} + h_4\{B_{s4}\}^T\{B_{s4}\})\{N]\}\,\mathrm{d}x \tag{A.4}$$

with matrices $[B_w]$, $[B_u]$, $\{B_{s2}\}$ and $[B_{s4}]$ given by

$$[B_w] = \left(\sum_{j=1,3,5} EI_j\right)\begin{bmatrix} 0 & 0 & 0 & 0 & 0 \\ 0 & 0 & 0 & 0 & 0 \\ 0 & 0 & 0 & 0 & 0 \\ 0 & 0 & 0 & 0 & 0 \\ 0 & 0 & 0 & 0 & 1 \end{bmatrix}, [B_u] = \begin{bmatrix} ES_1 & 0 & 0 & 0 & 0 \\ 0 & ES_3 & 0 & 0 & 0 \\ 0 & 0 & ES_5 & 0 & 0 \\ 0 & 0 & 0 & 0 & 0 \\ 0 & 0 & 0 & 0 & 1 \end{bmatrix}, \tag{A.5}$$

$\{B_{s2}\} = \{1\ \ -1\ 0\ 0\ d_2\}/h_2$ and $\{B_{s4}\} = \{0\ 1\ \ -1\ 0\ d_4\}/h_4$.

APPENDIX B. NOMENCLATURE

H	magnetic field
j	current density or unit vector for y direction
B	magnetic induction
M	magnetization
m	direction of magnetization
μ_0	permeability in vacuum
μ_r	relative permeability
E_m	magnetic energy
A	magnetic potential
V	volume of magnetic domain
i	unit vector for the x direction

$\mathbf{k}$	unit vector for the z direction
α_m	angle defining the direction of the magnetization
b	off-plane width of the magnetic domain
G	area of the magnetic domain
$[N_m]$	magnetic shape functions
$[D]$	matrix of nodal co-ordinates
$[K_m]$	magnetic stiffness matrix
α^e	magnetic domain element area
$\{Mg\}$	magnetization vector
$F_{m_s}^{(st)}$	static component of the magnetic force in the s direction
$F_{m_s}^{(d)}$	dynamic component of the magnetic force in the s direction
γ	shear strain
u	longitudinal displacement
w	vertical deflection
h	layer thickness
$\{\delta^e\}$	vector of generalized nodal displacements
$\{u\}$	vector of generalized element displacements
$[i]$	matrix of structural nodal coordinates
$[N]$	structural shape functions
U	strain energy
T	kinetic energy
W_e	work done by external forces
W_m	work done by magnetic forces
E	Young's modulus
A	area of cross-section
L	element length
G	shear modulus
I	second moment of area
$[M]$	mass matrix
ρ	density
$[K]$	stiffness matrix
$\{F\}$	load vector
$\{b\}$	vector for localization of the magnetic forces
$[K_{sm}]$	magneto-elastic coupling matrix
$[K_{dm}]$	magneto-structural stiffness matrix